Smart Structures and Systems, Vol. 4, No. 2 (2008) 153-169
DOI: http://dx.doi.org/10.12989/sss.2008.4.2.153

Experimental and numerical studies toward the implementation of shape memory alloy ties in masonry structures

Sara Casciati*

ASTRA Department, School of Architecture, University of Catania, Siracusa, Italy

Karim Hamdaoui

Department of Structural Mechanics, University of Pavia, Pavia, Italy

(Received October 4, 2006, Accepted August 8, 2007)

Abstract. The use of pre-tensioned shape memory alloy (SMA) wires to retrofit historic masonry structures is investigated. A small wall, serving as a prototype masonry specimen, is constructed to undergo a series of shaking-table tests. It is first studied in its original state, and its dynamic characteristics (in terms of modal frequencies) are extracted from the recorded signals. The results are then compared with those obtained when an increasing number of couples of pre-stressed SMA wires are introduced in the specimen to link the bricks together. A three-dimensional finite element model of the specimen is developed and calibrated according to the modal parameters identified from each experimental test (with and without SMA wires). The calibration process is conducted by enhancing the masonry mechanical behaviour. The results and the effectiveness of the approach are presented.

Keywords: masonry; numerical modelling; shaking table tests; shape memory alloys; system identification.

1. Introduction

When developing innovative techniques for the structural rehabilitation of historical buildings, the difficulties and the special requirements related to these types of structures must be considered. From a structural point of view, historical buildings can be cynically regarded as an assemblage of compact and un-reinforced stone elements, which are either connected by means of a weak mortar layer, or simply held together by gravity. Two main challenges are usually encountered: (i) the material properties are not directly estimable, and the constitutive law shows a nonlinear behaviour under the existing stress-state; (ii) the damage and construction history spans centuries, thus making the current structural assessment quite difficult. Furthermore, standard restoration techniques often result inadequate and fail to meet the non-invasive requirement.

Typologies, materials, and design techniques can significantly differ from a case to another. However, a common feature is the sensitivity to the vibrations induced by the surrounding environment and/or the natural hazards. This observation suggests to exploit the special features of the SMA (shape memory alloys) super-elastic behaviour under dynamic excitation. Pre-stressed SMA wires or trusses can be

*Assistant Professor, Corresponding Author, E-mail: saracasciati@msn.com

installed between the brick components, with the effects of limiting the relative displacements and, at the same time, dissipating energy (Casciati and Faravelli 2004). The ties are pre-tensioned up to the stress level which characterizes the "plateau" of the alloy constitutive law, so that the value of the linking prestressing force is preserved at an increased strain level.

A specific Copper-based alloy was identified as particularly suitable for the envisioned application, due to its low cost and its wide temperature range. Five years of experimental tests have provided a deep understanding of its mechanical behaviour (Casciati and Faravelli 2003, Casciati and Faravelli 2004, Casciati and Faravelli 2007), including the response to fatigue cycles (Casciati, *et al.* 2007, Casciati 2007).

The potential offered by this innovative retrofitting technique is the topic of several research studies performed within the European Union funded projects: ISTECH, MANSIDE, CHIME, and WIND-CHIME. Exhaustive reports of the achieved results can be found in Auricchio, *et al.* (2001), Cardone, *et al.* (1998), Casciati and Osman (2004), Casciati (2006). The effect of installing SMA devices on masonry structures was empirically evaluated, without a thorough attempt to investigate the mechanical principles that underlie the collected data.

The rationale governing the mechanics of the proposed retrofit technology is often hidden, in the literature, by either the results of laboratory tests or the sophisticated numerical models. The need to preliminarily model, plan, and optimize a retrofit operation via SMA devices led the authors of this paper to design and implement a step by step process, to be applied during the design phase of the retrofit.

The basic component is the brick or stone block. The tested specimen is made of a set of these components. First, the behaviour of the specimen during shaking table tests is analyzed. The results are then compared with the effects of introducing SMA retrofitting elements. The advantages of deploying the proposed pre-stressed SMA wires in the restoration of historical monuments are, finally, illustrated with reference to the standard technique of using steel bars. Only a summary of the main results is provided in this paper. The interested reader is referred to a Master thesis (Delmonte 2007) for the entire dataset.

In order to be considered as reliable, the quantitative results must, however, be updated on a case-specific basis, by collecting the measurements from the whole structural system mounting the SMA devices.

2. Single brick characterization

The experimental tests carried out within the research activity reported in this paper required the preliminary acquisition of a stock of bricks from the market. The geometry of a single brick is simply $25 \times 12.5 \times 5.5$ cm (slightly bigger than the nominal dimensions), and its mass density is $\rho = 1750$ kg/m^3. A Poisson ratio of 0.15 is assumed. A material specimen of sizes $2.5 \times 2.4 \times 2.5$ cm was cut from one of the bricks, in order to undergo a mono-axial compression test using the available universal testing machine. The sensor readings in 1 suggest an average value of the Young modulus equal to 916 MPa, with a peak value of 935 MPa. However, the test results are affected by the specimen reduced dimensions (scale effect), the brick porosity, and the testing conditions.

To improve the Young modulus estimate, a further test is performed on a sample brick. The brick is vertically mounted on a steel base, and supports a steel plate with a mass on the top. The resulting system is a single degree-of-freedom oscillator which is placed on a shaking table. Its resonant frequency is estimated for different mass values. A synthesis of the result is given in Table 1.

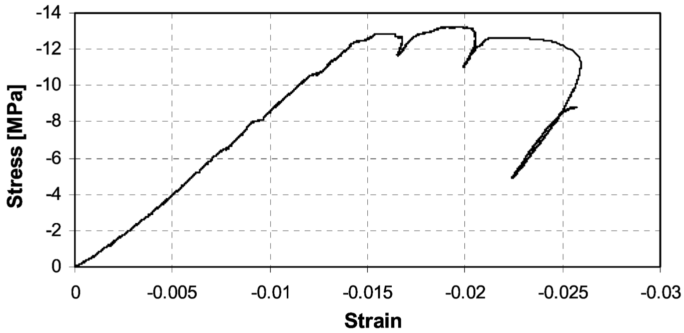

Fig. 1 Stress-strain diagram from the compression test (i.e. negative stress values) on the material specimen obtained from a single brick

Table 1 Estimates of the system natural frequency resulting from two shaking table tests on a single brick

Case #	Mass [kg]	Peak bottom acceleration [m/s^2]	Resonant frequency[Hz]	Young modulus estimate [kPa]
1	31	0.477	16.02	1078469.24
2	70	0.0703	10.03	1020597.74

3. The masonry specimen

A set of bricks is assembled to form a typical masonry specimen (Figs. 2 and 3). The specimen has the depth of two bricks (b = 25 cm), two bricks length (L = 50 cm), and the height of six layers of bricks (33 cm). The weight, P, is 0.6 kN. A rigid steel plate of mass 50 kg and thickness 2 cm is mounted on its top, in order to ideally simulate the weight of an upper wall portion. As a secondary effect, the rigid plate avoids the out-of-plane collapse of the system during the vibrations of low intensity. In the following calculations, a height h of 34 cm (including half of the steel plate) is considered.

The model is tested using the uni-axial shaking table available at the Vibration Laboratory of the Structural Mechanics Department, University of Pavia. Two accelerometers are mounted on the shaking table and on the top of the wall, respectively. A no-contact, laser optic sensor is also deployed to measure the displacements, but its readings are reliable only for large excitation intensities. Each single brick forming the masonry wall is of the same kind investigated in the previous section.

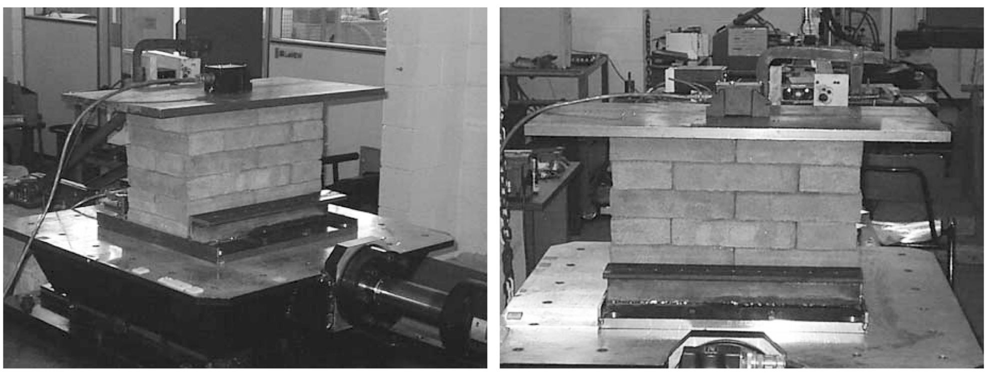

Fig. 2 The masonry specimen mounted on the shaking table

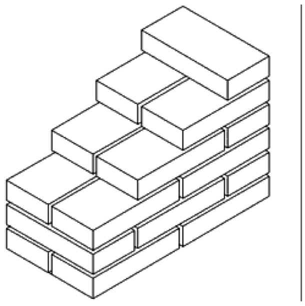

Fig. 3 Details of the tested wall

Table 2 Experimental frequencies detected by using the "N4Sid" state space algorithm. The equivalent Young modulus is then estimated from the homogeneous material numerical model (FEM)

Case	Excitation intensity factor	Shaking table peak acceleration [m/s^2]	Estimated parameters		
			Experimental Frequency [Hz]	FEM Equivalent Young Modulus [Mpa]	FEM Lumped Mass [kg]
1	0.1	0.04	11.10	9.480	96.95
2	0.5	1.44	8.74	5.875	96.91
3	1	4.79	8.73	5.865	96.96
4	1.25	7.13	6.45	3.200	96.92
5	1.875	10.17	4.78	1.758	96.95
6	2.5	12.35	4.60	1.628	96.94

3.1. Laboratory tests

The shaking table is driven by assigning the displacement time history obtained from a realization of a filtered white noise acceleration. Six tests are performed by multiplying the excitation displacement intensities by six different factors; namely: 0.1, 0.5, 1, 1.25, 1.875, and 2.5, respectively. The corresponding peak values of the recorded accelerations are reported in Table 2. The lack of linearity in their relation (very low peak accelerations are achieved when the intensity factor is either 0.1 or 0.5) depends on the response spectrum features of the available shaking table. The first series of tests aim to identify the wall original behaviour. Table 2 summarizes the results in terms of resonant frequencies, which are estimated by using the Matlab "N4Sid" State space algorithm (Matlab 2004).

In terms of graph, Fig. 4 shows a singular peak value in correspondence of the detected frequency. It is worth noticing that the second "hill" at 20 Hz is due to the resonance of the testing machine, and not to the tested specimen. The test with the excitation signal of highest intensity had to be interrupted before its scheduled duration, due to the excessive brick openings.

3.2. Finite element model and equivalent homogeneous material

In the standard finite element idealizations of masonry structures, a homogeneous and isotropic material model is adopted, with both compressive and tensile strengths different from zero. The elastic modulus of the so called "equivalent" material is fixed in such a way that the system under investigation behaves consistently with the actual experimental response, as suggested in El Borgi, *et al*. (2005).

Within the SAP 2000 software (version 9), three-dimensional, eight-node, solid elements are selected

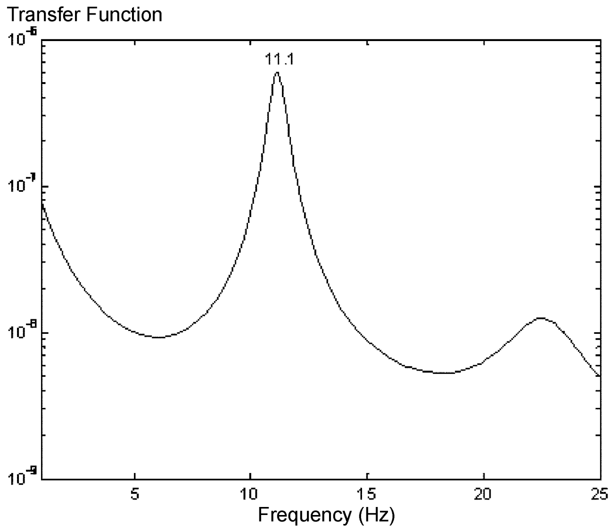

Fig. 4 Natural frequency of the un-reinforced masonry wall, as detected from the transfer function estimated by the excitation signal of the lowest intensity

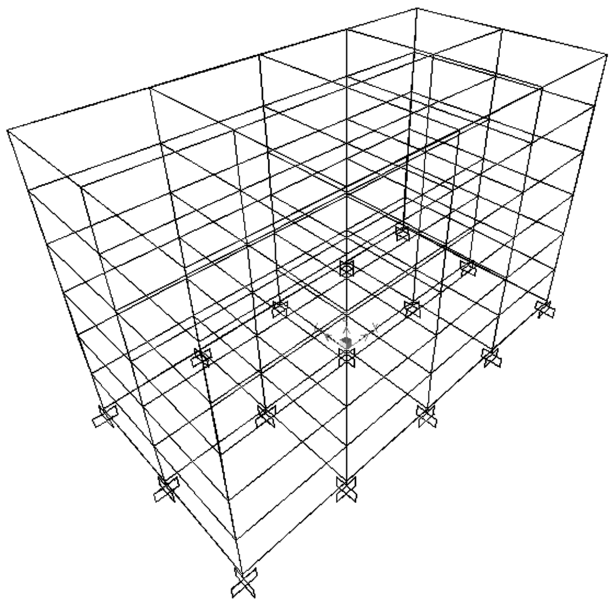

Fig. 5 Three-dimensional, eight-node, finite elements model of the masonry wall

to create a finite element model (FEM) of the wall specimen, as shown in Fig. 5.

The rigid plate mass is schematized by assigning lump masses to the nodes at the top of the mesh. As mentioned above, the material is assumed to be homogeneous and the modulus of normal elasticity is set equal to an "equivalent" value, E_{eq}, which is selected so that the analyses lead to detect the same natural frequencies obtained from the experimental tests. In Table 2, a different value of E_{eq} is found for each considered experimental test. The simple cantilever scheme in Fig. 5 has the stiffness properties governed by the following relation.

$$k = \frac{3E_{eq}J}{h^3} \tag{1}$$

being J the weak moment of inertia of the wall constant cross-section. By re-calculating the lumped mass of the top nodes as

$$m_L = \frac{(2\pi f)^2}{k} \tag{2}$$

approximately the same value is obtained for all the analyzed cases, as indicated in Table 2.

3.3. Accounting for a reduced effective cross-section

In the previous Section, different values of the masonry equivalent Young modulus, E_{eq}, were estimated from excitation signals of increasing intensities (Table 2). The present Section is dedicated to show that the dependence of E_{eq} on the excitation amplitude is only fictitious, being the differences in the experimental frequencies related to the geometrical changes of the masonry cross-section under the excitations of highest intensities.

In the absence of mortar, indeed, each brick can rotate around the three spatial axes, giving rise to openings as the ones in Fig. 6. This behaviour is un-respectful of the continuity assumption on which the beam theory relies. Thence, Eq. (1) is just an approximation.

The openings between two bricks, one over-standing the other, prevent to transmit the tensile stresses between them to the adjacent bricks, thus implying the inability of the cross-section to react under traction. As a consequence, the specimen effective cross-section is reduced to the compressed zones, whose width b_c is computed as follows.

The goal is to build the structural scheme of a cantilever beam with variable cross-section (Fig. 7). Under dynamic excitation, the effect of the rigid plate mass lumped at the top, together with the wall mass, is represented by an inertial force, $F = m_L a$, with a the horizontal acceleration at the top of the wall. The weight of the rigid plate also results in a centred axial load, N_{top}, acting on the free edge of the wall. The resultant of F and N_{top} is aligned with the mid-point of the cross-section width, b. Thus, at the free edge, the cross-section is fully compressed.

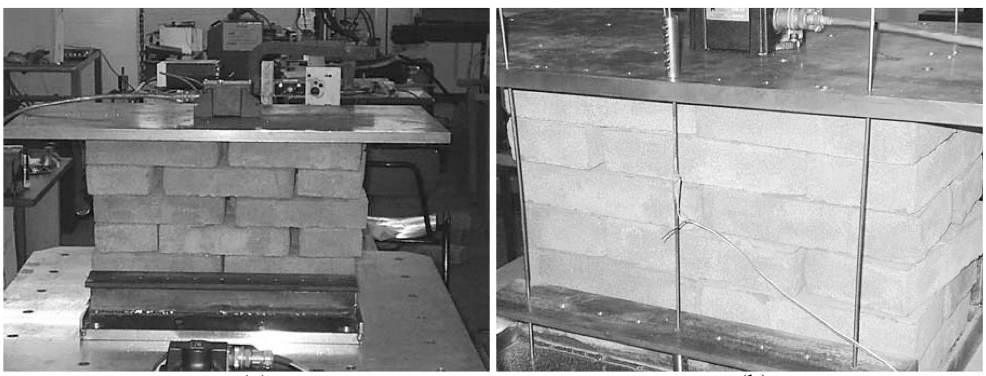

(a) (b)

Fig. 6 Examples of the brick openings at the end of the tests with the shaking table: (a) lateral displacements; (b) twisting around the vertical axis

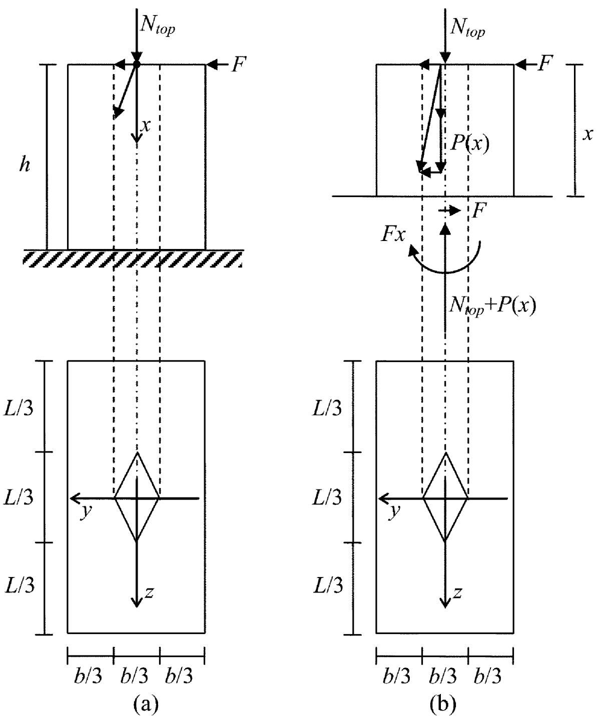

Fig. 7 The cantilever beam model and the inertial properties of its cross-section: (a) fully resistant section at top; (b) free body diagram of the wall upper portion

Let x denote the spatial coordinate that follows the beam axis, from the free edge to the bottom. Along x, the axial load gradually increases due to the self-weight of the increasing wall portion, $P(x) = \rho gA \cdot x$, where $g = 9.81$ m/s^2 is the gravity acceleration, and $A = bh$. From the free-body diagram of Fig. 7, the moment balance around the free edge requires that, at level x, the eccentricity $e(x)$ of the total axial force is given by

$$e(x) = \frac{Fx}{N_{top} + P(x)} \tag{3}$$

For $e(x) \le b/6$, the wall cross-section is fully reacting, being it subjected to only compressive stresses.

If h_c is the height at which the eccentricity $e(x)$ reaches the value of $b/6$, for $x > h_c$ the effective cross-section starts reducing due to the rising of tensile stresses. Within the range $b/6 < e(x) < b/2$, the depth, $b_c(x)$, of the compressed zone is given by

$$b_c(x) = 3\left(\frac{b}{2} - e(x)\right) \tag{4}$$

and it results from assuming a triangular re-distribution of stresses, whose resultant is aligned with the pressure point.

If x becomes greater than the level h_c^* at which $e(x) = b/2$, the wall cross-section is fully non reactive. The survival of the system is due to the dynamic nature of the excitation, while a static force would have caused the overturning of the wall.

The resulting moment of inertia, $J(x)$, of the effective cross-section has the following distribution along the beam axis

$$J(x) = \begin{cases} \frac{1}{12} L b^3 & \text{for } 0 < x < h_c \ (0 \le e(x) \le b/6) \\ \frac{1}{12} L \cdot [b^3(x)]^3 & \text{for } h_c < x < h_c^* \ (b/6 < e(x) \le b/2) \\ 0 & \text{for } h_c^* < x < h \ (b/2 < e(x)) \end{cases} \tag{5}$$

In a static context, the stiffness. k_F, against the horizontal force at the top, F, can be estimated by assuming an elastic behaviour for the cantilever beam of variable cross-section. Indeed, its inverse, $1/k_F$, that represents the flexibility associated with a given value of the force F, is computed as the displacement of the free edge under an unitary force, $F = 1$. For the numerical calculations, when $x > h_c^*$, a constant value slightly greater than zero is assigned to $J(x)$ The value of the Young modulus also needs to be a priori known. In the following, one assumes that it is equal to the value of the equivalent Young modulus, E_{eq}, estimated from the test with the excitation of low intensity. The lower values estimated from the other tests can be considered just as the results of an artifice to account for the actual inertial moment reductions, when they are not explicitly included in the analyses.

When the excitation of low intensity is considered, the masonry cross-section is fully reactive along the entire height of the structure, and the stiffness k is given by Eq. (1), since no openings are forming. The corresponding flexibility is constant and equal to $1/k$.

In the intermediate cases, where the maximum eccentricity is kept within the range ($b/6$, $b/2$), $J(x)$ is also a function of time, and the actual behaviour of the wall consists of alternating fully reactive states with the formation of openings, and viceversa. The nonlinear behaviour causes the tangent flexibility to vary from $1/k$ to $1/k_F$, with F the current level of the horizontal force. Reference can be made to Fig. 8, which plots the flexibility as a function of the top force F. For a given force $\bar{F}$, the area under the graph within $0 \le F \le \bar{F}$ is the static displacement under the force $\bar{F}$. The wall secant stiffness, k_{sec}, associated with this maximum value of the force is the ratio between the force and the area.

The test on the shaking table is of a dynamic nature, but the spectral analysis performs a linearization by identifying a sort of equivalent secant stiffness k_c, as different from the secant stiffness k_{sec} associated with the maximum value of the force. Therefore, the identified stiffness k_c will assume an intermediate value between the static secant stiffness, k_{sec}, and the one computed by Eq. (1) for a fully reacting cross-section. Once k_c is determined, the system frequency can be re-calculated by the equivalent of Eq. (2).

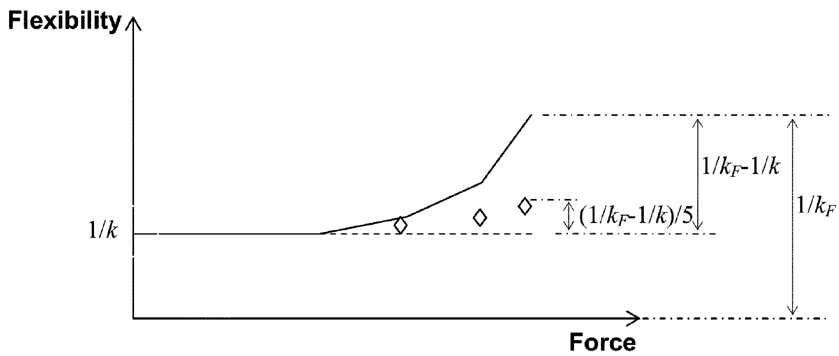

Fig. 8 Flexibility versus force

Table 3 Justification of the detected frequencies by simple geometry modifications (the values in italic were obtained by interpolation, they were not the results of a test): $N_{top} = 0.5$ kN

Shaking table peak acceleration [m/s^2]	Top peak acceleration [m/s^2]	Maximum Eccentricity [m]	b_c [m]	$10^4 J_{min}$ (at bottom) [m^4]	h_c [m]	k_c [kN/m]	Recalculated Frequency [Hz]	Experimental Frequency [Hz]
0.039	0.1170	0.0035	0.25	6.51	0.34	471.09	11.1	11.10
		< *b*/6				**Eq.(1)**		
0.52	1.388	0.0417	0.25	6.51	0.34	471.09	11.1	-
		= *b*/6				**Eq.(1)**		
1.44	2.846	0.085	0.119	0.71	0.1022	282.65	8.60	8.74
		< *b*/2	3			**= 0.6*k***		
4.79	4.406	> *b*/2	0	0.01	0.0590	272.25	8.43	8.73
7.13	4.289	> *b*/2	0	0.01	0.0607	180.35	6.87	6.45
10.17	5.108	> *b*/2	0	0.01	0.0495	116.47	5.52	4.78
12.35	4.757	**> *b*/2**	0	0.01	0.0537	70.66	4.30	4.60
						= 0.15*k*		

Empirically, one finds a good agreement with the experimental frequencies of Table 2 when k_c is estimated from the flexibility curve of Fig. 8, after reducing its ordinates by a factor of 1/5 in the range of F exceeding the linear field. This observation holds for excitation intensities that cause a maximum eccentricity within the range $b/6 < e(x) < b/2$. From the test results, within this range the value of k_c does not exceed an upper bound equal to $\alpha\, k$, with k given by Eq. (1) and α coefficient lower than one, whose value depends on the height h_c of the actually reacting part of the cantilever beam.

For excitations of higher intensities, a stiffness lower bound of $\beta\, k$, with β also depending on h_c, is experimentally found. Therefore, a linear interpolation between $\alpha\, k$ and $\beta\, k$ can be performed for the intermediate cases.

The results are summarized in Table 3, which reports, in the third row, a reduction of the fixed-edge effective cross-section that corresponds to $\alpha = 0.6$. The last row of Table 3 refers to the excitation of highest intensity. Since the associated test was interrupted because of failure, its results cannot directly be compared with the others. However, a stiffness lower bound with $\beta = 0.15$ is identified. A linear interpolation on the base accelerations is performed for the intermediate cases.

There is a satisfactory agreement between the values in the last two columns of Table 3. This supports the arguing that the equivalent Young modulus to be used for the analyses simply depends on the stress associated with the dead load, while the modifications emphasized as the shaking excitation increases are induced by geometrical matters. Furthermore, in view of the next tests, it is worth noticing a progressive decrease in terms of frequency (but with excellent benefit in terms of peak acceleration) as soon as the eccentricity reaches its upper value of $b/2$.

4. Adding SMA ties

4.1. Test setup and experimental results

The laboratory tests described in Section 3.1 are now repeated on the masonry specimen mounting the SMA ties. The selected alloy is labelled AH140 and it is supplied by the French company

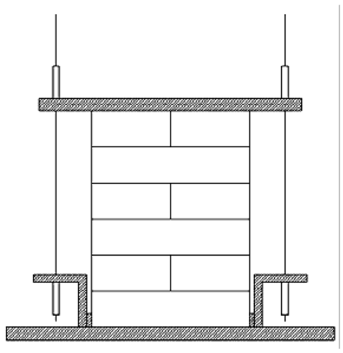

Fig. 9 Cross-section of the tied wall

Trefilmetaux. Its chemical composition, in weight percentage, is given as follows: Al = 11.8% ; Be = 0.5%; Cu = 87.7%. The following values of the transformation temperatures were provided by the producer:

$$M_s = -18\ ^{\circ}\mathrm{C};\ M_f = -47\ ^{\circ}\mathrm{C};\ A_s = -20\ ^{\circ}\mathrm{C};\ A_f = 2\ ^{\circ}\mathrm{C}$$

where "*M*" and "*A*" denote the martensite and the austenite, respectively, and "*s*" and "*f*" stays for "start" and "finish", respectively. The SMA devices are subjected to a preliminary thermal treatment (Casciati, 2007). A pre-tension is then given to the wires that are installed along the wall longitudinal sides (Fig. 9). An increasing number of couples of wires is considered by mounting: (a) a central wire on each of the opposite sides; (b) a wire at each specimen corner; and (c) three equidistant wires on each of the opposite sides.

The results gathered by applying the "N4Sid" state space algorithm to the recorded signals are summarized in Table 4, for all the considered structural configurations and excitation amplitudes.

Two considerations have to be made:

• When using only two SMA wires, the test with excitation of highest intensity causes the wires to fail;

• The excitation of lowest intensity produces signals whose amplitudes are so low that the machine resonance (at 20 Hz) corrupts the estimate of the system modal parameters. The Fourier transform plot in Fig. 10, which refers to the case of six wires, gives evidence to the latter statement. As a consequence, the values in the first row of Table 4 are disregarded by the following elaborations, while the values in the second row are assumed as frequency estimates for the case of fully reacting cross-section.

Table 4 Resonant frequencies of the tied specimen, as computed by"N4Sid"

Case	Excitation intensity	Detected frequencies [Hz]			
		Without SMA	With 2 SMA	With 4 SMA	With 6 SMA
1	0.1	11.10	≡	≡	≡
2	0.5	8.74	15.46	15.79	16.95
3	1.0	8.73	13.56	13.77	16.00
4	1.25	6.45	13.40	13.76	15.69
5	1.875	4.78	12.84	13.57	15.49
6	2.5	4.60	-13.66	15.02	

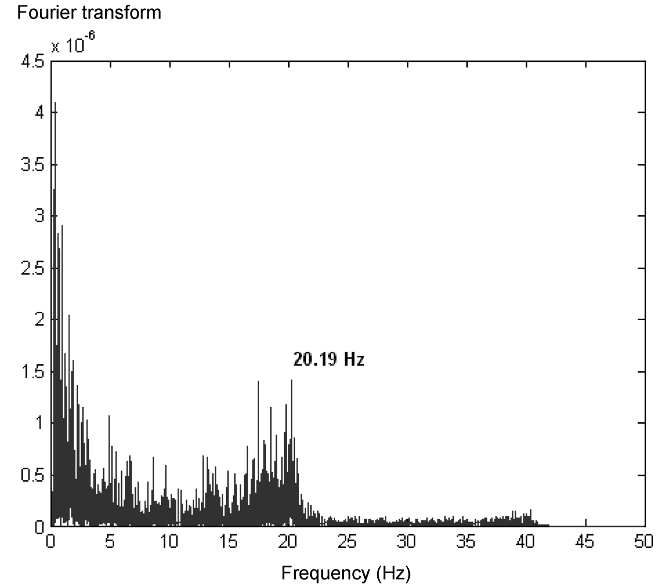

Fig. 10 Fourier transform of the top acceleration, showing the interaction between the wall frequency and the testing machine resonance

4.2. Elaboration of the numerical model

In the 3D, 8-node, solid finite elements model of the wall discussed in Section 3.2, the pre-tensioning effect of the SMA wires is simulated by applying compressive forces at the top of the model. In other words, when working on the plateau of the alloy constitutive law, no structural elements need to be introduced in order to model the wires presence; only couples of forces are considered at the application points. Fig. 11(a), 11(b), and 11(c) show the finite element model with the forces corresponding to the cases of two, four, and six SMA wires, respectively.

At the measured strain level of 4%, the stress in the SMA wires is about 250 MPa, and it falls approximately in the middle of the super-elastic plateau. In order to simulate the corresponding compressive effect on the masonry wall, a value of 1.59 kN per wire is assigned to the forces in Fig. 11.

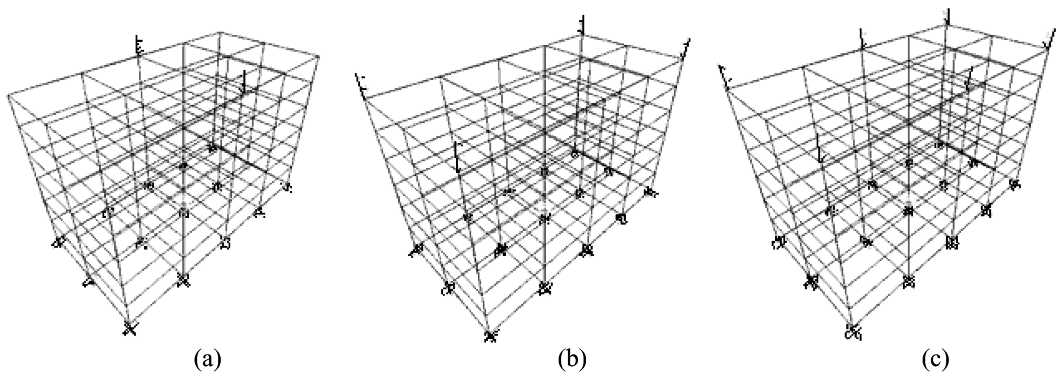

Fig. 11 Finite element model under different configurations of the compressive forces: a) 2 central forces, b) 4 forces at the corners, and c) 6 forces (3 equidistant forces on each side)

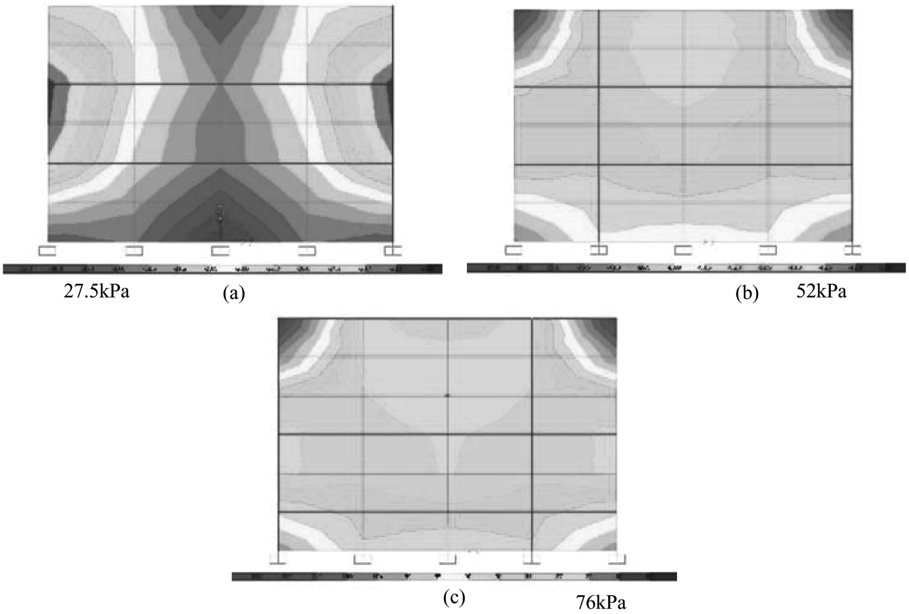

Fig. 12 Lateral view of the stress flow under the three loading conditions of Fig. 11: (a) two central forces, (b) four forces at the corners, (c) three equidistant on each side. The shown values are those of the stress at the medium level of the wall (they are marked below the corresponding colour in the pamphlet)

Fig. 12 shows a lateral view of the vertical component of the stress flow in the masonry wall, under the three considered loading conditions. For the cases using a number of SMA wires greater than two, Fig. 12(b) and 12(c) show a quiet homogeneous distribution of the stress induced by the pre-stressed ties. Conversely, in Fig. 11(a), the maximum stress values are reached only in the vicinity of the applied loads. Therefore, when only two wires are used, the regions in the vicinity of the devices must be distinguished from the rest of the structure.

4.3. Modal analyses accounting for the effective cross-section

The improvement due to the pre-stressing effect is now simulated by changing the equivalent modulus of elasticity, E_{eq}, of the wall. Once again, the aim is to achieve the same natural frequencies detected from the experimental tests (Table 5).

The calculations described in Section 3.3 are repeated with N_{top} accounting for the additional pre-tension force. The results are organized in the Tables 6, 7, and 8 for the three cases of 6, 4, and 2 wires,

Table 5 Detected frequencies using N4Sid State space algorithm and equivalent Young modulus from the numerical model (FEM)

Number of SMA wires	Excitation intensity factor	Estimated parameters		
		Experimental Frequency [Hz]	FEM Equivalent Young modulus [Mpa]	FEM Lumped mass [kg]
2	0.5	15.46	18.59 (20.66+16.53)	98.03
4	0.5	15.79	19.18	96.94
6	0.5	16.95	22.10	96.91

Table 6 Justification of the detected frequencies by simple geometry modifications (the values in italic were obtained by interpolation): 6 SMA ties and N_{top} = (0.5 + 9.569) kN

Table peak acc. (test) [m/s^2]	Top peak acc. (test) [m/s^2]	Max Eccentricity [m]	b_c [m]	10^4 $J_{\min}$ (at bottom) [m^4]	h_c [m]	k_c [kN/m]	Re-estimated Frequency [Hz]	Experimental Frequency (test) [Hz]
0.078	0.078	0.0002 < ***b*/6**	0.25	6.51	0.34	1098.21 **Eq.(1)**	16.95	16.95
2.92	6.706	0.0209 < ***b*/6**	0.25	6.51	0.34	1098.21 **Eq.(1)**	16.95	16.95
5.84	13.9715	0.0417 = ***b*/6**	0.25	6.51	0.34	1098.21 **Eq.(1)**	16.95	-
6.82	21.237	0.0662	0.176	2.28	0.222	1061.80 > 0.75 *k*	16.67	16.00
8.24	25.655	0.0800	0.135	1.02	0.184	966.79 > 0.75 *k*	15.90	15.69
11.44	28.462	0.0887	0.109	0.54	0.166	879.59 > 0.75 *k*	15.17	15.49
13.84	31.153	0.0971	0.084	0.24	0.151	823.66 = **0.75 *k***	14.68	15.02

Table 7 Justification of the detected frequencies by simple geometry modifications (the values in italic were obtained by interpolation): 4 SMA ties and N_{top} = (0.5 + 6.380) kN

Table peak acc. (test) [m/s^2]	Top peak acc. (test) [m/s^2]	Max. Eccentricity [m]	b_c [m]	10^4 $J_{\min}$ (at bottom) [m^4]	h_c [m]	k_c [kN/m]	Re-estimated Frequency [Hz]	Experimental Frequency (test) [Hz]
0.117	0.117	0.0006 < ***b*/6**	0.25	6.51	0.34	1098.21 **Eq.(1)**	15.79	15.79
1.48	4.367	0.0209 < ***b*/6**	0.25	6.51	0.34	1098.21 **(Eq. 1)**	15.79	15.79
2.94	8.690	0.0417 = ***b*/6**	0.25	6.51	0.34	1098.21 **Eq.(1)**	15.79	-
4.40	16.726	0.0801	0.135	1.02	0.183	826.89 > 0.75*k*	14.70	13.77
5.65	20.625	0.0988	0.079	0.20	0.147	714.83 = **0.75*k***	13.67	13.76
8.69	23.861	0.1143	0.032	0.014	0.133	714.83 = **0.75*k***	13.67	13.57
9.47	24.095	0.1154	0.029	0.01	0.125	714.83 = **0.75*k***	13.67	13.57

Table 8 Justification of the detected frequencies by simple geometry modifications (the values in italic were obtained by interpolation): 2 SMA ties and N_{top} = (0.5 + 3.19) kN

Table peak acc. (test) [m/s2]	Top peak acc. (test) [m/s2]	Max. Eccentricity [m]	b_c [m]	10^4 $J_{\min}$ (at bottom) [m^4]	h_c [m]	k_c [kN/m]	Re-estimated Frequency [Hz]	Experimental Frequency (test) [Hz]
0.078	0.078	0.0004 < ***b*/6**	0.25	6.51	0.34	1098.21 **Eq.(1)**	15.46	15.46
1.48	3.938	0.0356 < ***b*/6**	0.25	6.51	0.34	1098.21 **Eq.(1)**	15.46	15.46
3.46	4.667	0.0417 = ***b*/6**	0.25	6.51	0.34	1098.21 **Eq.(1)**	15.46	-
4.44	13.139	0.118	0.019	0.01	0.123	693.03 = **0.75*k***	13.39	13.56
5.77	16.882	> *b*/2	0	0.01	0.095	664.99	13.18	13.4
7.44	19.027	> *b*/2	0	0.01	0.083	601.81	12.96	12.84

respectively. In Tables 6 and 7, is equal to 0.75 and the eccentricity is always lower than its upper limit.

In Table 8 (only two SMA wires), the eccentricity reaches the upper limit, α is equal to 0.75, and β is fixed at 0.6. For the case in which the wall is retrofitted by only two SMA wires (one on each longitudinal side), the simulation process is still pursued by changing the modulus of elasticity of the wall, E_{eq}, but a value of (1.25 E_{eq}) is used to enhance the characteristics of the wall region near the wires emplacement. The E_{eq} value is, instead, assigned to the regions far away from the central wires, as suggested by Fig. 12(a). Indeed, the stress distribution reported in this figure shows in the middle higher

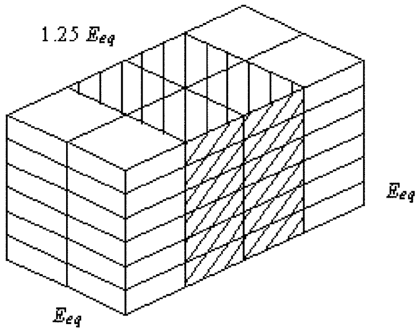

Fig. 13 Central zone (dashed) with 1.25 E_{eq}, and lateral zones with E_{eq}

values than laterally, and the ratio between the relevant stresses is about 1.25. Fig. 13 illustrates the areas characterized by different values of the equivalent Young modulus. Conversely, Fig. 12(b) and 12(c) justify the assumption of a uniform distribution of E_{eq} in the entire wall specimen, for the cases where more than two wires are used.

4.4. Discussion

A three-dimensional diagram is given in Fig. 14. It explains the relationship between the experimental frequencies obtained using different excitation amplitudes, and the number of wires used in the retrofit of the studied masonry wall.

The developments of this paper have emphasized that the dependence of E_{eq} on the vibration intensity is fictitious, because it is a consequence of the inability of the masonry to sustain tensile stresses. If this

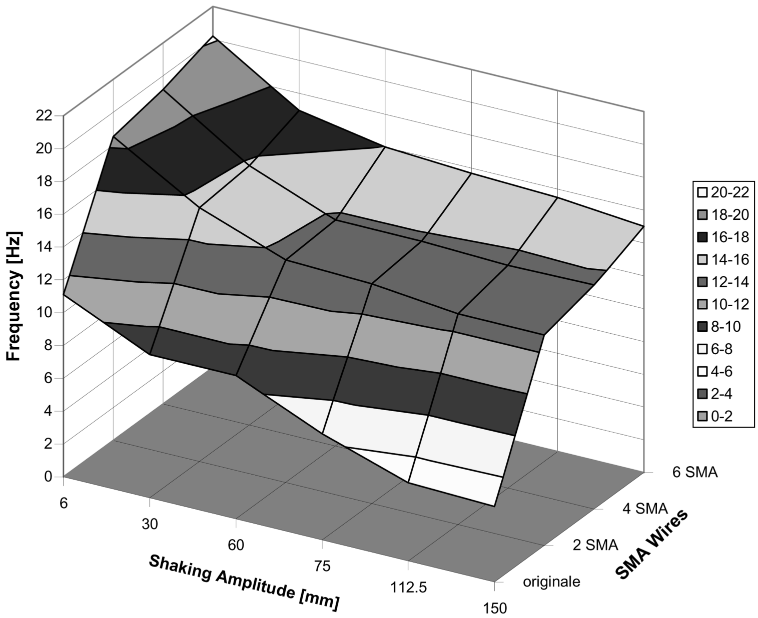

Fig. 14 Three-dimensional representation of the frequency vs. the amplitude and number of wires according to the experimental tests

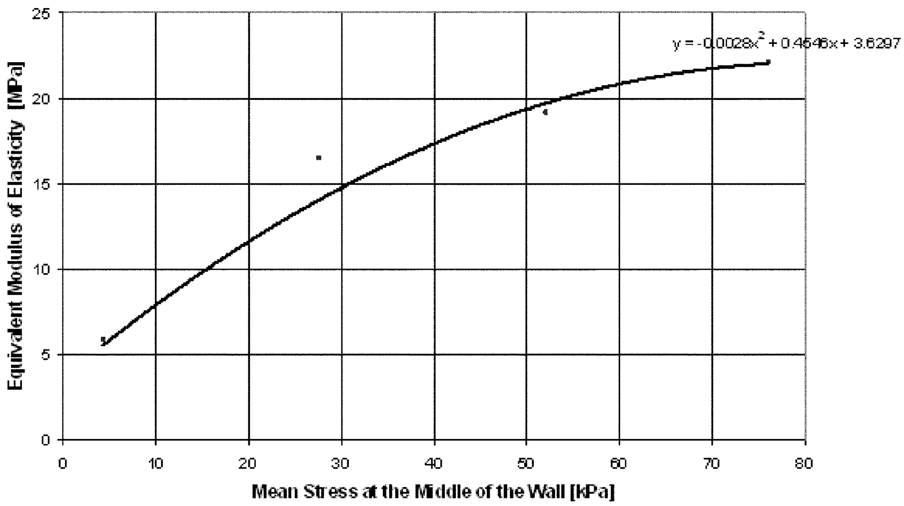

Fig. 15 Equivalent modulus of elasticity vs. the stress in the wall for the cases of fully reacting section

aspect is directly taken into account by considering the reduced moment of inertia of the effective cross-section, a constant equivalent Young modulus can be assumed in the analyses, independently of the applied excitation intensity.

The graph of Fig. 15 reports the variation of the equivalent modulus of elasticity E_{eq} versus the average stress in the wall (see Fig. 8). The interpolation is achieved by a second order polynomial equation.

The retrofitting not only improves the masonry behaviour by increasing the value of the equivalent Young modulus, but it also plays a very significant role in delaying any sort of progressive failure, thus providing to the structure the feature of robustness.

4.5. Comparison of using SMA versus steel ties

The response of the wall FEM incorporating the SMA ties under 20% of El-Centro earthquake, applied in the weak direction, is evaluated. In order to compare the effects of using steel instead of SMA ties, the analyses are repeated by inserting "link" elements at the same locations of the compressive forces in Fig. 11. Under the assumption that the steel wires provide the same compressive effect as the SMA ties, the values of the masonry equivalent Young modulus are still the ones identified in Table 5. However, the steel devices not only enhance the structural performance by exerting linking forces, but they also increase the structural stiffness. To account for both these effects, it is necessary to actually insert in the wall mesh additional elements modeling the steel devices and acting as elastic springs. For this purpose, the steel elastic properties (E = 210 MPa) are assigned to "link" elements of length l = 33 cm and diameter Φ = 3 mm. The resulting additional stiffness per wire is given by:

$$k_{(1\ \text{steel wire})} = \frac{E\pi\Phi^2}{l} = 4498.19\ \text{kN/m} \tag{7}$$

The number of wires and their placement reflect the three retrofitting scenarios envisioned when using SMA ties. The results, obtained for the lowest excitation amplitude that led to reliable results (second row of Table 5), are collected in Table 9 and compared to the corresponding cases using SMA ties. In

Table 9 SMA ties vs. steel ties

Structural Configuration	E_{eq} [kPa]	Frequencies with SMA [Hz]	Frequencies with steel [Hz]	Max. displacement with SMA [mm]	Max. displacement with steel [mm]
Original	5875	8.739	8.739	4.457	4.457
2 wires	20665	15.461	16.847	1.514	1.305
4 wires	19180	15.789	17.938	1.463	0.919
6 wires	22100	16.949	20.542	1.151	0.811

particular, the system natural frequency and the maximum displacement at the wall top, in the same direction of the excitation, are reported. The driving excitation is now the 1940 El-Centro accelerogram scaled by 20%. When adopting steel wires, larger frequencies and smaller displacements are found with respect to the corresponding cases using SMA ties. As expected, a stiffer behavior of the wall is achieved by adding steel elements, with negative effects in terms of energy dissipation.

5. Conclusions

Ancient constructions often present themselves as simple assemblages of masonry blocks. It is a common practice to sew them by metallic ties, which are usually pre-tensioned. The main drawback is the rising of inelastic permanent deformations under high intensity excitations.

This paper discusses the design aspects related to the adoption of ties in shape memory alloy. The results of laboratory tests drive the development of a numerical model incorporating the effects of the SMA devices. First, the structure is analyzed in its original state, without any retrofit attempt. The effects of several retrofitting solutions are then experimentally evaluated and included in the numerical model by accordingly changing the equivalent Young modulus. The response under 20% of 1940 El Centro accelerogram is compared to the ones of the initial structure and the structure mounting steel ties, in order to quantify the effectiveness of the retrofit and its advantages with respect to traditional techniques.

In conclusion, ties of shape memory alloy (SMA) in austenitic phase offer three main benefits:

a) By prescribing that the assigned pre-tension must reach the plateau of the super-elastic constitutive law, no additional stress is transferred to the masonry at higher strain levels. Therefore, no springs need to be added to the numerical model, with consequent possibility of mutual displacements between the masonry blocks, i.e., energy dissipation;

b) Further energy dissipation is achieved by the hysteresis loop of the hyper-elastic stress -strain relation (Auricchio, *et al*. 2001);

c) The ties are able to re-centre themselves in the initial position, without any residual displacement.

Acknowledgements

The research activity summarized in this paper was supported by the FP6 European project WIND-CHIME. For some specific activity, the Italian research project supported by the National Research Council (CNR), with Prof. Di Tommaso of the School of Architecture in Venice serving as coordinator, is also acknowledged.

References

Auricchio, F., Faravelli, L., Magonette, G. and Torra, V. (Eds.) (2001), *Shape Memory Alloys: Advances in Modelling and Applications*, CIMNE, Barcelona.

Cardone, D. Dolce, M and Nigro, D. (1999), "Experimental test on SMA based seismic devices", *Proceedings of MANSIDE Project Final Workshop*, Rome.

Casciati, F. (2006), "Structural monitoring for the diagnostic and the retrofitting of the monumental heritage", *Proceedings of Structural Health Monitoring and Intelligent Infrastructures*, Shenzen University, Taylor and Francis, London, 49-54.

Casciati, F. and Faravelli, L. (2004), "Experimental characterization of a Cu-based shape memory alloy toward its exploitations in passive control devices", *Journal de Physique IV*, **115**, 299-306.

Casciati, F., Casciati, S. and Faravelli, L. (2007), "Fatigue characterization of a Cu-based shape memory alloy", *Proceedings of the Estonian Academy of Sciences – Physics Mathematics*, **56**(2), 207-217.

Casciati, S. (2007), "Thermal treatment optimization for Cu-based shape memory alloys", *Proceedings of the First International Conference on Self-healing Materials,* Noordwijk, April.

Casciati, S. and Faravelli, L. (2003), "Thermo-mechanic properties of a Cu-based shape memory alloy", *Proceedings of SMART03*, Warsaw.

Casciati, S. and Faravelli, L. (2007), "Structural components in shape memory alloy for localized energy dissipation", *Computer & Structures*, [accepted for publication].

Casciati, S. and Osman, A. (2005), "Damage assessment and retrofit study for the Luxor Memnon Colossi", *J. Struct. Control Health Monitoring*, **12**(2), 139-156.

Delmonte, G. (2007), *Pretensionamento con Fili in Lega a Memoria di Forma di Elementi Strutturali Murari*, Master Thesis (in Italian), Department of Structural Mechanics, University of Pavia, Italy.

El-Borgi, S., Choura, S., Ventura, C., Baccouch, M. and Cherif, F. (2005), "Modal identification and model updating of a reinforced concrete bridge", *J. Smart Struct. Sys.*, **1**(1), 83-101.

Matlab (2004), Version 7 (R14) [computer program], The MathWorks Inc., *http://www.mathworks.com*.

FC